Generation of slow waves in the antral region of guinea-pig stomach – a stochastic process

G. D. S. Hirst and F. R. Edwards

Department of Zoology, University of Melbourne, Victoria 3010, Australia

(Received 2 February 2001; accepted after revision 6 April 2001)

1. Slow waves were recorded from the circular muscle layer of the antral region of guinea-pig stomach. Slow waves were abolished by 2APB, an inhibitor of IP_3-induced Ca^{2+} release.

2. When the rate of generation of slow waves was monitored it was found to vary from cycle to cycle around a mean value. The variation persisted after abolishing neuronal activity with tetrodotoxin.

3. When simultaneous recordings were made from interstitial cells in the myenteric region (ICC_{MY}) and smooth muscle cells of the circular layer, variations in the rate of generation of slow waves were found to be linked with variations in the rate of generation of driving potentials by ICC_{MY}.

4. A preparation was devised which consisted of the longitudinal muscle layer and ICC_{MY}. In this preparation ICC_{MY} and smooth muscle cells lying in the longitudinal muscle layer generated driving potentials and follower potentials, synchronously.

5. Driving potentials had two components, a rapid primary component that was followed by a prolonged plateau component. Caffeine (3 mM) abolished the plateau component; conversely reducing the external concentration of calcium ions $[Ca^{2+}]_o$ mainly affected the primary component.

6. Analysis of the variations in the rate of generation of driving potentials indicated that this arose because both the duration of individual driving potentials and the interval between successive driving potentials varied.

7. It is suggested that the initiation of pacemaker activity in a network of ICC_{MY} is a stochastic process, with the probability of initiating a driving potential slowly increasing, after a delay, from a low to a higher value following the previous driving potential.

Contractions of the gastrointestinal tract are associated with a discharge of slow waves in the muscle layers: these occur at low frequencies in the absence of stimulation (Tomita, 1981; Sanders, 1992). Slow waves are initiated by interstitial cells of Cajal (ICC), not by smooth muscle cells (Thuneberg, 1982; Sanders, 1996). Intestinal preparations taken from mutant mice which lack myenteric ICC (Ward *et al.* 1994; Huizinga *et al.* 1995) or ones in which the development of ICC has been impaired (Ward *et al.* 1997, 1999; Ordog *et al.* 1999) fail to generate slow waves. Myenteric ICC (ICC_{MY}) in the guinea-pig antrum generate large amplitude, long lasting, depolarizing membrane potential changes, termed driving potentials. Driving potentials spread passively to both the longitudinal and circular muscle layers. In the circular muscle layer, the depolarization produced by each driving potential gives rise to the initial phase of each slow wave. The initial phase triggers a regenerative response in the circular muscle layer, resulting in a complete slow wave (Dickens *et al.* 1999; Suzuki & Hirst, 1999; Edwards *et al.* 1999; van Helden *et al.* 2000). The regenerative component of the slow waves depends upon the presence of intramuscular ICC (ICC_{IM}); it is absent in gastric muscles from mutant mice devoid of ICC_{IM} (Dickens *et al.* 2001). In the longitudinal muscle layer, which lacks ICC_{IM}, the depolarizations produced by driving potentials fail to trigger a regenerative component like that generated in the circular muscle layer. In the longitudinal muscle layer the potential changes generated in ICC_{MY} produce passive waves of depolarization, termed follower potentials, which in turn activate L-type calcium channels (Dickens *et al.* 1999, 2000).

Pacemaker ICC have been isolated from the intestine of mice (Tokutomi *et al.* 1995; Thomsen *et al.* 1998; Koh *et al.* 1998) and from the submucosal pacemaker region of the dog colon (Lee & Sanders, 1993). Individual murine intestinal ICC_{MY} generate an ongoing discharge of pacemaker activity even when the cells are voltage clamped with their membrane potentials held at negative

values (Tokutomi *et al.* 1995; Thomsen *et al.* 1998; Koh *et al.* 1998). This, and other observations, has led to the suggestion that pacemaker activity involves the cyclical release of calcium ions (Ca^{2+}), from internal stores in concert with mitochondrial Ca^{2+} uptake (Ward *et al.* 2000*b*). Pacemaker activity also involves the activation or participation of an inositol trisphosphate (IP_3), receptor since slow waves are absent in gastric muscles of mutant mice which lack IP_3-type 1 receptors (Suzuki *et al.* 2000).

ICC_{MY} have not been isolated from the stomach and little is known about how they generate rhythmical activity. Some aspects of the way in which pacemaker activity is generated by gastric ICC_{MY} may differ from the way activity is generated by intestinal ICC_{MY}. In the mouse intestine slow waves occur at a frequency of some 20 to 30 waves per minute (Ward *et al.* 1994) whereas in the stomach they occur at three to five waves per minute (Dickens *et al.* 2001). Furthermore individual intestinal slow waves are much briefer than are those recorded from the stomach (Ward *et al.* 1994; Dickens *et al.* 2001). In this report we describe some of the properties of driving potentials recorded from the network of ICC_{MY} lying in the antral region of the guinea-pig stomach. It is suggested that driving potentials consist of two components, a primary voltage-dependent component that propagates through the network of ICC_{MY} and a plateau component that is triggered by the primary component. A hypothesis is presented which suggests that pacemaker activity is initiated in a stochastic manner with the dominant pacemaker region shifting through the network of ICC_{MY}.

METHODS

The procedures described have been approved by the animal experimentation ethics committee at the University of Melbourne. Guinea-pigs of either sex were stunned, exsanguinated and the stomach removed. In all experiments the antrum was dissected free and immersed in oxygenated physiological saline (composition; mM): NaCl, 120; $NaHCO_3$, 25; NaH_2PO_4, 1.0; KCl, 5; $MgCl_2$, 2; $CaCl_2$, 2.5; and glucose, 11; bubbled with 95 % O_2–5 % CO_2. In the initial experiments the mucosa was removed and the preparations were pinned out in a recording chamber serosal-surface uppermost as described previously (Dickens *et al.* 1999). Intracellular recordings were made using sharp microelectrodes (90–150 MΩ) filled with 0.5 M KCl and conventional recording techniques (Dickens *et al.* 1999). In some experiments a single microelectrode was used to record from the circular muscle layer. In other experiments, two independently mounted microelectrodes were used to record simultaneously from ICC_{MY} and the circular muscle layer. In the second series of experiments, preparations of antral longitudinal muscle were prepared in the same way as has been described previously for duodenal preparations (Hirst *et al.* 1974). These preparations were pinned out in a recording chamber with the serosal surface downwards. When viewed with an inverted microscope the preparations were found to retain the myenteric plexus. In many experiments freshly dissected preparations were incubated with an antibody to Kit (Anti-Murine Kit (ACK-2); Gibco BRL, Life Technologies, Paisley, Scotland, UK, diluted 1 in 500 in physiological saline) for 15 min. After this the preparations were washed with oxygenated physiological saline for 15 min. Subsequently the preparations were incubated with a secondary antibody labelled with a fluorescent tag (Alexa-488; Molecular Probes, Eugene, OR, USA, diluted 1 in 500 in physiological saline) for 15 min. After washing for a further 15 min with physiological saline, preparations were viewed with a fluorescence microscope. The preparations retained a network of ICC_{MY} but ICC_{IM} could not be detected in the longitudinal muscle layer. In some experiments a single electrode was used to record from either ICC_{MY} or the longitudinal muscle layer. In other experiments, two independently mounted microelectrodes were used to record simultaneously from ICC_{MY} and the longitudinal muscle layer. During each experiment either preparation was constantly superfused with physiological saline solution warmed to 37 °C; nifedipine (1 μM) was added to the physiological saline to reduce the amplitudes of the rhythmical contractions associated with each driving potential. All data are expressed as means ± standard error of the mean (S.E.M.). Student's *t* test was used to determine if data sets differed, with P of < 0.05 regarded as significant.

The time courses of individual unitary potentials (see Fig. 6*B*) were described by the difference between two exponential functions raised to the third power using the relationship $(e^{-t/A} - e^{-t/B})^3$ (for further details see Edwards *et al.* 1999). Spectral densities (see Fig. 7) were estimated as described previously (Edwards *et al.* 1999). Briefly the square of the magnitude of the fast Fourier transform (FFT) of sequences of between 512 and 120 000 points of sampled data was taken. The straight line of best fit to the data was first subtracted from each sequence to remove any monotonic trends in voltage that occurred during the repolarization phases of driving potentials. Means of the FFTs of eight data sequences were taken to improve the estimate of spectral density. Theoretical fits to spectral density curves were obtained by assuming that they were made up of randomly occurring shot particles with time courses described by the difference between two exponential functions raised to the third power. The standard deviation about the mean of membrane potential occurring before the upstroke or after the repolarization phase of strings of driving potentials (see Fig. 11) was determined as described previously (Edwards *et al.* 1976).

Drugs used in this study were nifedipine, tetrodotoxin, caffeine, indomethacin (Sigma Chemical Co., St Louis, MO, USA) and 2-aminoethoxydiphenyl borate (2APB, Calbiochem, San Diego, California, USA).

RESULTS

General observations

When intracellular recordings were made from the antral region of the guinea-pig stomach the same three distinct patterns of rhythmical electrical activity which have been described previously (Dickens *et al.* 1999) were detected. Approaching from the serosal surface, the first cells impaled generated follower potentials. Follower potentials had amplitudes of some 15 to 35 mV and maximum rates of rise (dV/dt_{max}) of less than 0.1 V s^{-1}; the cells generating such signals have previously been identified as smooth muscle cells lying in the longitudinal layer (Dickens *et al.* 1999). After passing through the longitudinal layer, cells were occasionally impaled, which generated large amplitude driving potentials. Driving potentials had amplitudes in excess of 40 mV and maximum rates of rise (dV/dt_{max}) in excess of 0.1 V s^{-1}; it has previously been shown that driving potentials are generated by ICC_{MY} (Dickens *et al.* 1999). In the circular muscle layer an ongoing discharge of slow waves was detected. Slow waves, which

had initial and secondary components, had peak amplitudes of some 25 to 40 mV (see Dickens *et al.* 1999).

In many rhythmically active tissues the activity results from the cyclical activation of voltage-dependent channels (see as examples Noble, 1984; Anderson, 1993). In contrast, slow waves generated in the different regions of the murine gastrointestinal tract appear to involve Ca^{2+} release from internal stores and IP_3 receptors (Ward *et al.* 2000*b*; Suzuki *et al.* 2000). This view was tested in the guinea-pig antrum by adding 2APB, an agent which blocks IP_3-dependent Ca^{2+} release (Maruyama *et al.* 1997), to the physiological saline. When this was done, slow waves were reduced in amplitude, their durations became briefer and eventually they were abolished (Fig. 1). In this series of experiments, control slow waves had peak amplitudes of 31.1 ± 1.6 mV and half-widths of 5.67 ± 0.52 s; these were superimposed on peak negative potentials of -67.0 ± 1.4 mV ($n = 5$; mean ± S.E.M.; in this and every other case each n value refers to an observation made on a separate preparation). In solutions containing 2APB (20 μM) slow waves had peak amplitudes of 24.4 ± 1.2 mV and half-widths of 4.64 ± 0.58 s, superimposed on peak negative potentials of -61.5 ± 1.9 mV ($n = 5$). In solutions containing 2APB (40 μM) slow waves had peak amplitudes of 15.0 ± 3.0 mV and half-widths of 2.89 ± 0.80 s, superimposed on peak negative potentials of -58.8 ± 2.8 mV ($n = 5$). In each of these experiments the responses that persisted had amplitudes similar to the initial component of the slow wave, perhaps indicating that the secondary component of the slow wave was more sensitive to 2APB than the primary component. In solutions containing 2APB (60 μM) all electrical activity was abolished and the steady negative potential was -57.0 ± 1.6 mV ($n = 5$). These observations support the view that IP_3 or IP_3-dependent Ca^{2+} stores are involved in the generation of gastrointestinal slow waves (Ward *et al.* 2000*b*; Suzuki *et al.* 2000).

When rhythmical activity results from the cyclical activation of voltage-dependent channels, the rate of generation of activity is constant, unless the nerves innervating the pacemaker region are activated (see for example Choate *et al.* 1993). In the antrum the rate of generation of slow waves fluctuated about a mean rate (Fig. 2*B*). In colonic tissues where the rate of generation of slow waves also varies, part of the fluctuation results from ongoing activity of enteric neurones and much of the variation is reduced by tetrodotoxin (TTX) (Sanders & Smith, 1986). In antral preparations, the addition of TTX (1 μM) to the physiological saline affected neither the mean rate nor the variability in rate of generation of slow waves. This was shown by measuring the distribution of time periods between the starts of successive slow waves. When this was done, the mean period of successive slow waves in control solution was 17.86 ± 1.95 s; in TTX-containing solutions the mean period was 18.49 ± 2.05 s ($n = 5$). Using a 2-tailed paired t test, these values were not significantly different, $P > 0.06$ ($n = 5$). Similarly variations in rate, determined from measurements of periodicity, were also unchanged. The mean standard deviation of periodicity determined in control solution was 1.95 ± 0.55 s and the mean standard deviation of periodicity determined in the presence of TTX was 2.05 ± 0.63 s, $P > 0.3$ ($n = 5$). Using the Wilcoxon-Mann-Whitney test, the distributions of periodicities were also found to be unchanged by the addition of TTX; in each case $P > 0.05$, ($n = 5$). The addition of TTX failed to change the peak negative potential recorded between slow waves: peak negative potential in control solution -68.4 ± 1.5 mV, after the addition of TTX, -68.2 ± 1.2 mV, $P > 0.7$ ($n = 5$). Similarly the amplitudes of slow waves were unchanged: the peak amplitude in control solution was 32.8 ± 0.8 mV; after the addition of TTX,

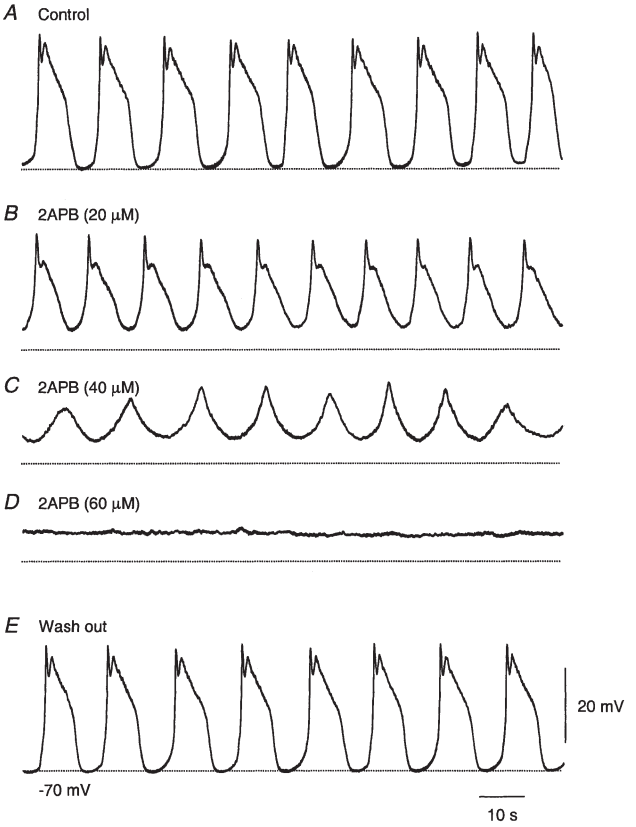

Figure 1. Effect of 2APB on slow waves recorded from the circular layer of the gastric antrum of a guinea-pig

The upper trace (*A*) shows successive slow waves recorded from the circular layer of the guinea-pig antrum in control solution. The peak negative membrane potential, illustrated with dotted line, was −70 mV. The subsequent traces (*B*, *C* and *D*) show recordings made from the same cell in the presence of 20, 40 and 60 μM 2APB, respectively. An equilibration period of 10 min was allowed between each recording after the addition of each concentration of 2APB to the physiological saline. The bottom recording (*E*) was made 15 min after washing with drug-free physiological saline. The time and voltage calibration bars apply to each recording.

the peak amplitude was 32.8 ± 0.6 mV, $P > 0.9$ ($n = 5$). In three experiments, indomethacin (10 μM) was added to the physiological saline, and again the variations in periodicity persisted. In eight preparations where the responses to inhibitory and excitatory nerve stimulation were abolished with apamin, L-nitro-arginine and hyoscine (see Dickens *et al.* 2000), the rate of discharge of slow waves varied from cycle to cycle.

Antral slow waves are initiated by driving potentials generated in ICC_{MY} (Dickens *et al.* 1999). To examine whether variations in the periodicity of slow waves resulted from changes in rate of generation of driving potentials, simultaneous recordings were made from ICC_{MY} and nearby circular smooth muscle cells. In each of six experiments, it was found that the rates of generation of both driving potentials and slow waves varied around the same mean rate (Fig. 2*A* and *B*). When individual slow waves were examined it was found that the onset of each driving potential coincided with the start of each slow wave and most of the rising phase of each driving potential preceded the initial component of each slow wave (Fig. 2*C*).

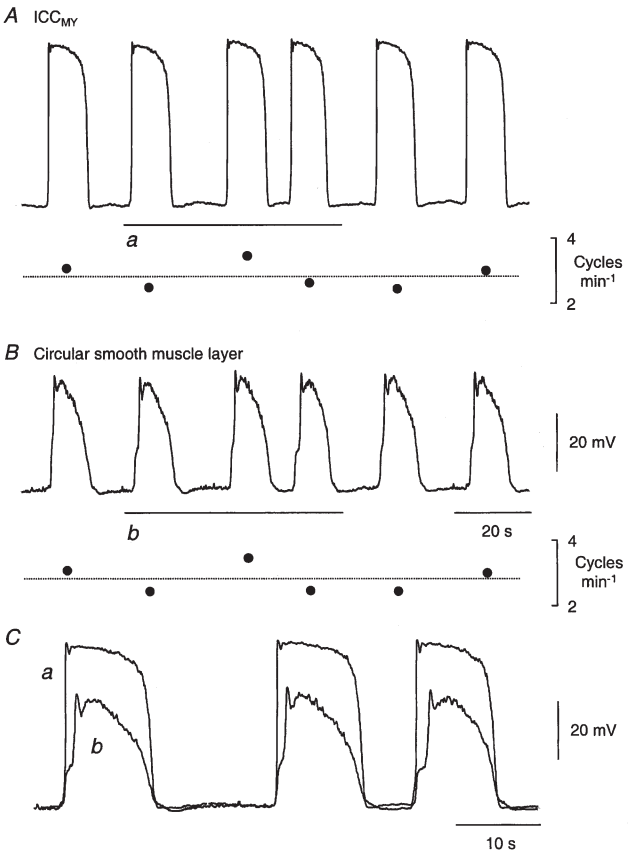

Figure 2. Simultaneous recordings of driving potentials and slow waves from antrum of guinea-pig

The upper trace (*A*) shows the discharge of driving potentials, along with a rate plot, recorded from a myenteric interstitial cell. The middle trace (*B*) shows the discharge of slow waves, along with its rate plot, recorded simultaneously from the circular layer, with the electrode within 50 μm of that used to record the driving potential. Regions of each trace (*a* and *b*) are expanded and overlaid in *C*. It can be seen that driving potentials and slow waves occurred synchronously (*C*). The upper voltage and time calibration bars apply to *A* and *B*. The lower voltage and time calibration bars apply to *C*. The peak negative potential of both cells was −65 mV.

Together the observations indicate that the rate of generation of slow waves varies from cycle to cycle. The variability does not result from ongoing neuronal activity generated in the myenteric plexus; rather it is associated with variations in the rate of occurrence of driving potentials initiated in ICC_{MY}.

Electrical properties of ICC_{MY} and longitudinal muscle cells

To simplify the interpretation of observations made on ICC_{MY}, preparations were further dissected by removing the circular muscle layer. These preparations had several advantages. Firstly since living ICC_{MY} could be labelled with an antibody to Kit along with a fluorescent secondary antibody, ICC_{MY} could be visualised and therefore more frequently impaled. Secondly since the preparations were thin, diffusional delays during solution changes should be reduced. Finally as ICC_{IM} were not found in these preparations any contribution such cells might make to rhythmicity was absent (see van Helden *et al.* 2000).

When recordings were made from these preparations two types of cells were detected. In one group of cells driving potentials were detected (Fig. 3*A*). Driving potentials again had peak amplitudes in excess of 40 mV and rapid rising phases. Each driving potential consisted of two components, a primary component and a plateau component (Fig. 3*A*). Follower potentials were detected from the other group of cells. These had peak amplitudes of less than 40 mV and slower rising phases than driving potentials. On most occasions a distinct primary component was not detected at the start of each follower potential (Fig. 3*B*) but occasionally such a component was apparent (see Fig. 4*C*). The properties of driving and follower potentials were compared in 12 preparations. The primary components of driving potentials had mean amplitudes of 44.5 ± 1.8 mV, and plateau components had mean peak amplitudes of 45.9 ± 1.7 mV and these were superimposed on peak negative potentials of −65.7 ± 0.9 mV. Follower potentials had peak amplitudes of 29.1 ± 2.1 mV and these were superimposed on peak negative potentials of −65.0 ± 0.7 mV. Using a 2-tailed paired *t* test, the peak amplitudes were found to be significantly different, $P < 0.001$; but the peak negative potentials recorded from the two cell types did not differ, $P > 0.08$. Driving potentials had a mean dV/dt_{max} of 0.34 ± 0.04 V s^{-1} whereas follower potentials had a mean dV/dt_{max} of 0.07 ± 0.01 V s^{-1}; these values were significantly different, $P < 0.001$. In each preparation, driving and follower potentials had similar half-widths and occurred at similar

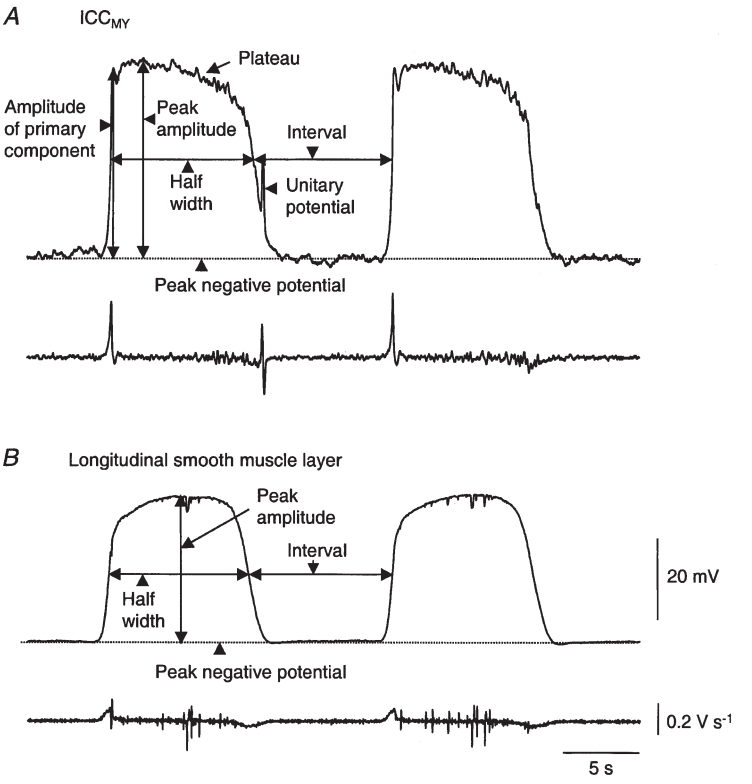

Figure 3. Driving potentials and follower potentials recorded from longitudinal muscle strips of the guinea-pig antrum

The upper pair of traces (*A*) show successive driving potentials and their derivatives. Note that the voltage recording contained discharges of membrane noise and that dV/dt_{max} of the primary component was about 0.4 V s^{-1}. The lower pair of traces (*B*) show successive follower potentials, along with their derivatives, recorded from the same preparation. When discharges of membrane noise occurred in this recording they were restricted to the regions where the membrane was depolarized and consisted of transient hyperpolarizations; dV/dt_{max} of the start of each follower potential was less than 0.1 V s^{-1}. The peak negative potential of both cells was −64 mV. The voltage, derivative and time calibration bars apply to both pairs of traces.

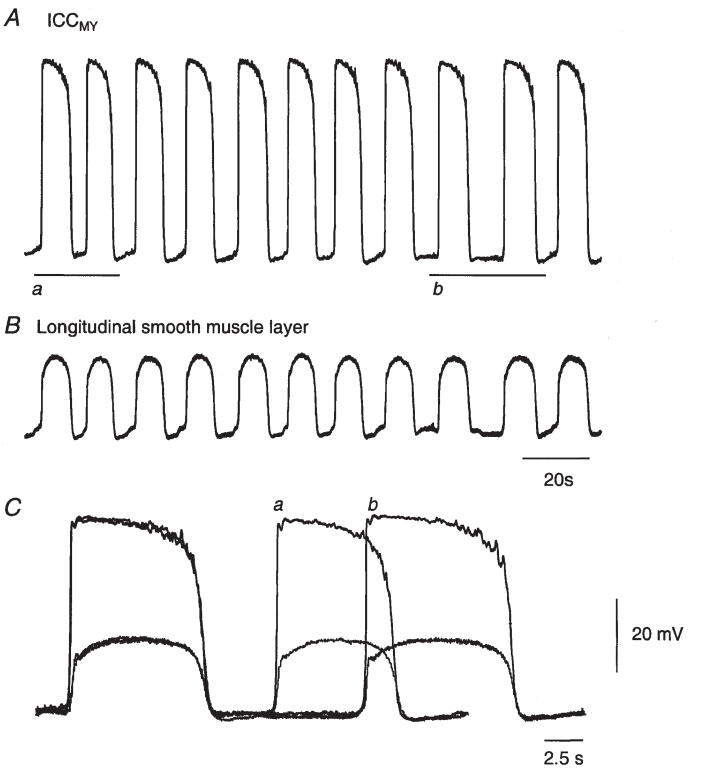

Figure 4. Simultaneous recordings of driving potentials and follower potentials from the longitudinal layer of guinea-pig antrum

The upper trace (*A*) shows the discharge of driving potentials recorded from a myenteric interstitial cell. The middle trace (*B*) shows the discharge of follower potentials recorded simultaneously from the longitudinal muscle layer, with the electrode within 50 μm of that used to record the driving potential. Bars *a* and *b* apply to traces *A* and *B* and are expanded and overlaid in *C*. It can be seen that driving potentials and follower potentials occurred synchronously but that the interval between successive pairs of potentials was not constant (*C*). Note also that when the interval between driving potentials was short, both the subsequent driving potential and the subsequent follower potential had briefer durations (*Ca*) than when preceded by a longer interval (*Cb*). The voltage calibration bar applies to all recordings. The peak negative potential of the interstitial cell was −63 mV and of the longitudinal muscle cell was −65 mV. The upper time calibration bar applies to *A* and *B*. The lower time calibration bar applies to *C*.

frequencies. The mean half-width of driving potentials was 8.84 ± 0.39 s, and that of follower potentials was 9.11 ± 0.40 s; these values were not significantly different, $P > 0.15$. The mean frequency of driving potentials was 3.66 ± 0.13 waves min^{-1}, and that of follower potentials was 3.85 ± 0.16 waves min^{-1}; these values were not significantly different, $P > 0.18$.

In 10 preparations, recordings were made using two independent microelectrodes. A longitudinal muscle cell was impaled and then the tissue was probed with the second electrode until an interstitial cell was impaled; the separation between electrodes was less than 60 μm. An experiment is illustrated in Fig. 4. In this and all other experiments, driving potentials and follower potentials occurred synchronously (Fig. 4*A* and *B*). The start of the upstroke of each driving potential was coincident with the start of the depolarisation detected in the longitudinal layer (Fig. 4*C*). Again much of the upstroke of the driving potential preceded the rising phase of the follower potential (Fig. 4*C*). In five of these experiments current pulses were passed through the recording electrodes used to impale the longitudinal muscle cells, in each case electrotonic potentials were detected in the nearby ICC_{MY}. In this group of experiments, driving potentials had a mean peak amplitude of 48.6 ± 1.4 mV, a mean dV/dt_{max} of 0.30 ± 0.05 V s^{-1} and a mean peak negative potential of −65.2 ± 1.4 mV. Follower potentials had a mean peak amplitude of 23.2 ± 2.3 mV, a mean dV/dt_{max} of 0.06 ± 0.01 V s^{-1} and a mean peak negative potential of −65.1 ± 0.7 mV. Using a 2-tailed paired *t* test, both the peak amplitudes and maximum rates of rise were found to be significantly different, $P < 0.001$ whereas the maximum negative potentials were found not to differ significantly, $P > 0.8$.

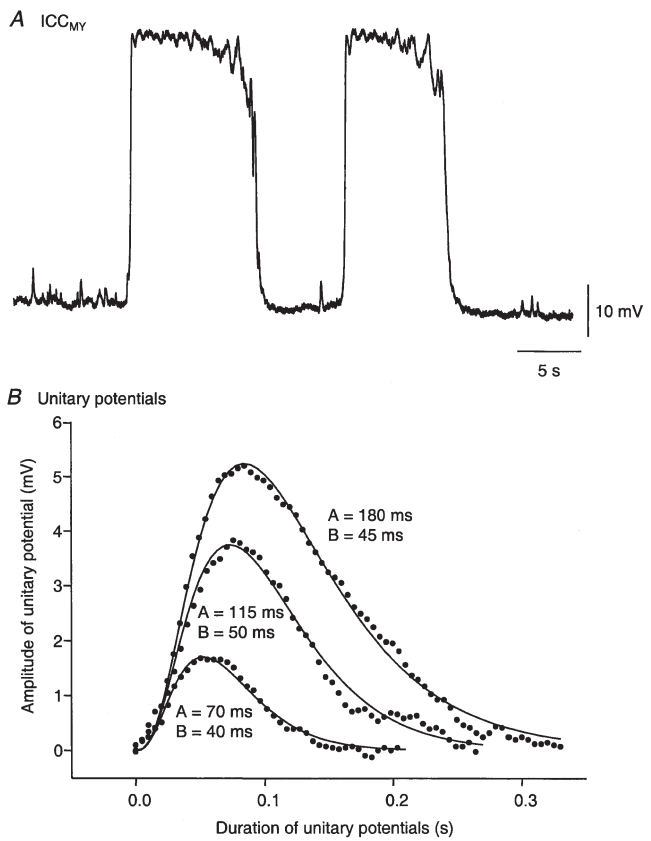

Figure 5. Discharge of unitary potentials during intervals between driving potentials

The upper trace (*A*) shows successive driving potentials recorded from an interstitial cell. It can be seen that in the intervals between driving potentials, discharges of unitary potentials were detected. Unitary potentials had variable amplitudes and did not occur immediately after the end of each driving potential. The peak negative potential of this cell was −65 mV. *B* shows theoretical fits of three unitary potentials selected for their range of amplitudes from the recording illustrated in *A*. The lines of best fit were calculated from the relationship $(e^{-t/A} - e^{-t/B})^3$ and the values of constants *A* and *B* used in each calculation are given with each curve. Data points (●) are shown.

Membrane potential recordings from ICC_{MY} and longitudinal smooth muscle cells differed in that those obtained from ICC_{MY} were often dominated by discharges of membrane noise. This was apparent during the plateau phases of driving potentials (Figs 3 and 4) and more rarely during the interval between driving potentials (Fig. 5). When detected during the interval between driving potentials, the noise was made up of bursts of transient depolarizations. Since these events have similar characteristics to those detected in isolated bundles of the circular layer of the guinea-pig antrum, the same terminology will be used; each transient depolarization will be termed a unitary potential (Edwards *et al.* 1999). Unitary potentials varied in amplitude both from preparation to preparation (compare Fig. 5*A* with Fig. 11*E*) and during a given recording (Fig. 5*A*). In the example shown in Fig. 5, unitary potentials ranged in amplitude from 0.2 to 9.8 mV, mean 2.0 ± 0.3 mV, $n = 50$, where on this occasion *n* refers to number of unitary potentials counted in this cell. Individual unitary potentials had total durations of some 150–400 ms, rise times in the range 30–190 ms, mean 60 ± 5 ms, and half-widths in the range 40 to 305 ms, mean 110 ± 9 ms ($n = 50$). In a group of ICC_{MY} where the characteristics of unitary potentials were measured, the mean amplitudes of unitary potentials ranged from 1.0 to 2.0 mV, mean 1.4 ± 0.2 mV ($n = 6$, where each *n* value again represents the mean amplitude of unitary potentials determined from a separate preparation). Their mean rise times lay in the range 35–145 ms, mean 75 ± 15 ms ($n = 6$). Their mean half-widths lay in the range 65–250 ms, mean 130 ± 25 ms ($n = 6$). When the time courses of individual unitary potentials were examined it was found that they could be described by the difference between two exponential functions raised to the third power (Fig. 5*B*). In the present experiments constant *A* had values in the

range 140–570 ms, mean 310 ± 65 ms, and constant B had values in the range 35–125 ms, mean 80 ± 15 ms ($n = 6$). These values are similar to those determined for unitary potentials recorded from bundles of circular muscle containing ICC_{IM} (Edwards *et al.* 1999).

In contrast, discharges of membrane noise were frequently absent in recordings from longitudinal muscle cells (Fig. 4). When present the membrane noise consisted of a few transient hyperpolarizing events which occurred during the follower potential (Fig. 3*B*).

Driving potentials and follower potentials could also be distinguished when the spectral characteristics of the two waveforms were determined. Power spectral-density curves, determined during the plateau component of driving potentials, had characteristic shapes (Fig. 6*A*). Energy increased from low values above 10 Hz to approach a plateau value near 1 Hz. At frequencies above 10 Hz, the power spectral-density curves became dominated by electrode recording noise (see Edwards *et al.* 1999). Power spectral-density curves, determined from isolated bundles of antral circular muscle containing ICC_{IM}, could be well described by assuming that the noise was made up of many unitary potentials (Edwards *et al.* 1999). When the same approach was taken with spectral-density curves obtained from ICC_{MY}, similarly good fits were obtained (Fig. 6*A*). In this series of experiments constant A had values in the range 255–670 ms, mean 455 ± 55 ms, and constant B had values in the range 25–45 ms, mean 35 ± 5 ms ($n = 6$). These values are similar to those determined from individual unitary potentials recorded from ICC_{MY}.

In contrast, an obvious plateau was not detected in any of the power spectral-density curves calculated from membrane potential recordings taken from longitudinal muscle cells ($n = 6$; Fig. 6*B*). Rather the curves were similar to those determined from recordings taken when the microelectrodes were in the physiological saline. As such the spectral-density curves obtained from longitudinal muscle recordings simply reflect the properties of the recording system.

Together these observations indicate that the simplified preparations contained both longitudinal smooth muscle cells and ICC_{MY}. The two cell types could be distinguished on electrophysiological grounds. Driving and follower potentials had different rates of rise, different amplitudes and different power spectral-density curves. Both cell types were coupled together into a common electrical syncytium but since characteristic membrane noise was only detected in ICC_{MY}, ICC_{MY} must generate it.

Driving potentials appeared to consist of two components, a primary component followed by a plateau component, with the two components of the driving potential having different sensitivities to caffeine. Caffeine (3 mM) caused a variable hyperpolarization, range 0–7 mV, mean 5.0 ± 0.6 mV, and abolished the plateau component (Fig. 7*A*). During the onset of the hyperpolarization, the duration of driving potentials was shortened (Fig. 7*Bb*) and eventually only the primary component remained (Fig. 7*Bc*). The abolition of the plateau component did not appear to be caused by the caffeine-induced hyperpolarization as primary components alone were frequently observed during washout of caffeine when the membrane potential had returned towards its resting value (Fig. 7*A*). In the control solutions, the primary component had a mean peak amplitude of 39.4 ± 2.5 mV, the plateau component had a peak amplitude of 45.6 ± 1.5 mV and the driving potential had a half-width of 8.36 ± 0.55 s

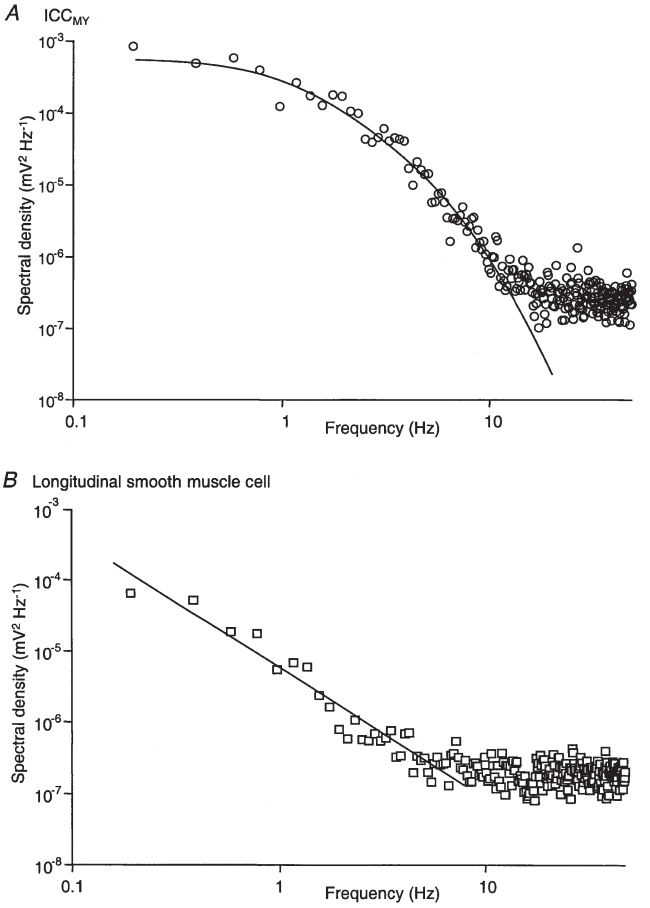

Figure 6. Spectral-density curves of membrane noise generated during plateaux of driving potentials and during follower potentials

The upper spectral-density curve (*A*) was calculated from eight successive plateau components of the driving potential illustrated in Fig. 4*A*. The set of data is fitted with a curve of best fit with time constants for A and B of 475 and 25 ms, respectively. The lower spectral-density curve (*B*) was calculated from eight successive follower potentials illustrated in Fig. 4*B*. The straight line is drawn by eye. Note the presence of an obvious plateau in the spectral-density curve calculated from the interstitial cell recording (*A*). A plateau was not apparent in the spectral-density curve calculated from the recording made from the longitudinal muscle cell (*B*).

($n = 5$). In the presence of caffeine, when the plateau had been abolished, the primary component had a mean amplitude of 40.1 ± 3.4 mV and a mean half-width of 0.81 ± 0.06 s ($n = 5$). In three of these experiments, caffeine (3 mM) was applied whilst simultaneous recordings were being made from ICC_{MY} and nearby longitudinal cells. In each case changes in the shape of the follower potential occurred synchronously with changes in the shape of the driving potential. As the plateau component of the driving potential shortened in the presence of caffeine, so the duration of the follower potential shortened. This observation is consistent with the view that follower potentials largely result from depolarizing current spreading passively from nearby ICC_{MY} (Dickens *et al.* 1999, 2000).

The time course of onset of the plateau component was estimated by subtracting the caffeine resistant primary component from driving potentials recorded in control solutions (Fig. 7*C*). When this was done, the onset of the plateau component was found to occur about 1 s, 0.94 ± 0.08 s ($n = 5$), after the onset of the primary component (Fig. 7*D*).

The two components of the driving potential were further distinguished when the concentration of calcium ions, $[Ca^{2+}]_o$, in the physiological saline was reduced (Fig. 8). Halving $[Ca^{2+}]_o$ reduced the maximum rate of rise of the driving potential and slightly reduced the peak amplitude of the primary component but did not change the amplitude of the plateau (Fig. 8*B*). A further halving of $[Ca^{2+}]_o$, further reduced the maximum rate of rise of the driving potential and in 3 of the 5 preparations examined, this reduction in $[Ca^{2+}]_o$ abolished the primary component (Fig. 8*C*). The grouped results from these experiments are shown graphically in Fig. 8*D*. Even when a primary component could not be detected, rhythmical activity persisted, albeit at a reduced rate (Fig. 8*C*). In four experiments (not illustrated) superfusing the preparations with nominally Ca^{2+}-free solutions abolished all rhythmical activity after some 5–7 min and caused a membrane depolarization of some 15–20 mV.

Pacemaker activity generated by ICC_{MY}

As has been pointed out variations in the rate of generation of slow waves resulted from variations in the rate of generation of successive driving potentials (Fig. 2). The instantaneous rate of generation and duration of successive driving potentials were determined from sequences of successive driving potentials, using the simplified preparations described above (Fig. 9*A*). The rate of generation of driving potentials varied around mean frequencies of some 3–5 waves min^{-1}; 3.3 ± 0.3 waves min^{-1} ($n = 6$) (Fig. 9*B*). Variations in the duration of individual driving potentials and in the interval between the end and start of a subsequent driving potential each contributed to the variability. When the

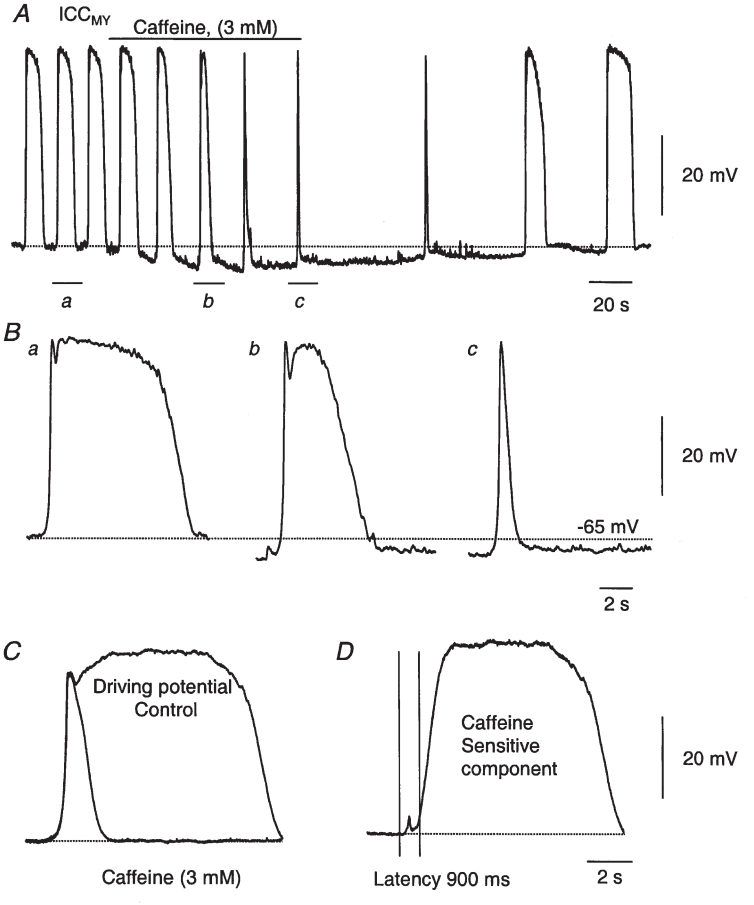

Figure 7. Effect of caffeine on a driving potential recorded from an ICC_{MY}

The upper trace (*A*) shows the effect of caffeine (3 mM) on the discharge of driving potentials. Caffeine increased the peak negative potential by some 4 mV and slowed the rate of occurrence of driving potentials. The driving potentials became briefer and occurred irregularly. As caffeine was washed out, the peak negative potential returned to its control value. After a delay, a slow discharge of long-lasting driving potentials was detected. When regions of the trace were displayed on an expanded time base (*B*), it could be seen that caffeine initially shortened the duration of the plateau component (*Bb*) and then abolished it (*Bc*). The pair of traces in *C* show a recording of a control driving potential superimposed on the primary component recorded in caffeine (3 mM). The trace in *D* shows the difference between the two traces. It can be seen that the plateau component starts some 900 ms after the onset of the primary component. These recordings were selected from a recording at a time when the peak negative potential was the same (−67 mV). The upper time calibration bar refers to the continuous recording (*A*), the middle time calibration bar refers to the expansions shown in *B* and the lower time calibration bar refers to *C* and *D*.

relationship between the half-width and subsequent interval was determined, a correlation was not detected. When lines of best fit were calculated, they had slopes near zero, mean slope -0.13 ± 0.50 ($n = 6$) and the fits had low regression coefficients, with a mean regression coefficient of -0.01 ± 0.50 (Fig. 9*C*). In contrast when the relationship between interval and subsequent half-width was determined, a correlation was found (Fig. 9*D*). The relationships were well fitted with straight lines, mean slope 0.31 ± 0.03, and each fit had a high regression coefficient, mean regression coefficient 0.97 ± 0.01 ($n = 6$). This observation indicates that the longer the interval between driving potentials then the longer the duration of the subsequent driving potential. On the other hand, the duration of a driving potential does not influence when a subsequent driving potential will occur. When a frequency histogram of the intervals between driving potentials was constructed it could be seen that driving potentials never occurred at intervals of less than 3 s and that the longest interval between successive

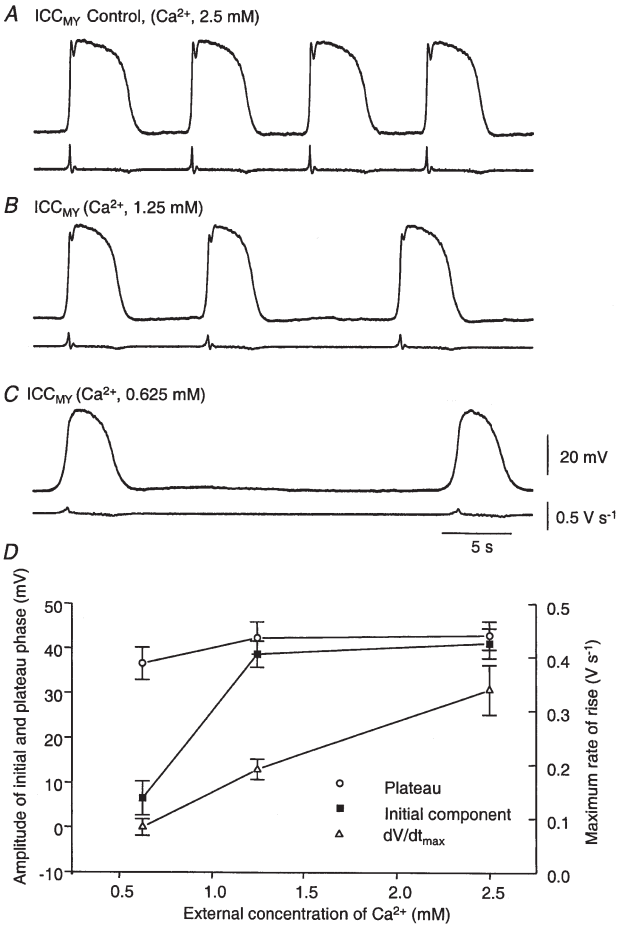

Figure 8. Effect of reducing $[Ca^{2+}]_o$ on driving potentials recorded from antrum of guinea-pig

The upper pair of traces (*A*) show a recording of control driving potentials along with their derivatives: peak negative potential −67 mV. Reducing $[Ca^{2+}]_o$ to half (*B*) caused the discharge to become irregular, slightly reduced the amplitude of the primary component and reduced dV/dt_{max}: peak negative potential −68 mV. A further halving of $[Ca^{2+}]_o$ (*C*) abolished the primary component of the driving potential, leaving an erratic discharge of plateau components: peak negative potential −65 mV. The grouped data from the experiments are shown in *D*. The time, voltage and dV/dt calibration bars apply to all recordings.

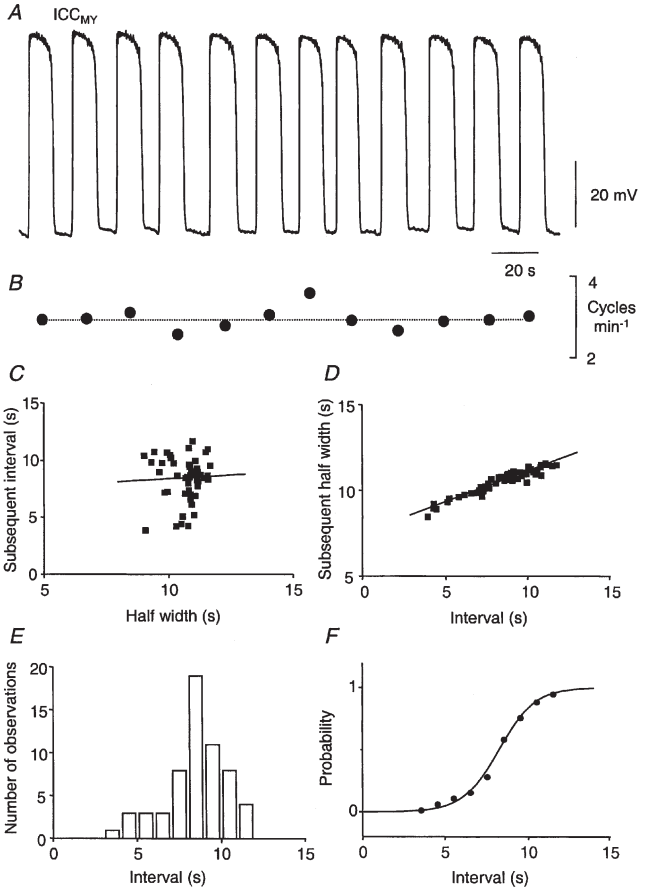

Figure 9. Irregular discharge of driving potentials generated by an interstitial cell of the guinea-pig antrum

The upper trace (*A*) shows the discharge of driving potentials: peak negative potential −69 mV. The rate of discharge (*B*) varied from cycle to cycle around a mean of 3.1 cycles min^{-1}. The relationship between half-width and subsequent interval (defined in Fig. 4*A*) is shown in *C*. It can be seen that the points were widely scattered around the line of best fit. The relationship between interval and subsequent half-width is shown in *D*. The data points are tightly clustered around the line of best fit. The frequency histogram of intervals is shown in *E*. It can be seen that the interval between driving potentials was always greater than 3 s and the most frequent interval was 8 s. The relationship between probability of initiation of a driving potential and interval length is given in *F*. The relationship was described by a Boltzmann sigmoidal expression. The time and voltage calibration bars apply to recording *A*.

driving potentials was some 12 s (Fig. 9*E*). This suggests that immediately after the end of each driving potential, regardless of its width, the probability that a subsequent driving potential will occur falls to zero; but after a delay, the probability that a subsequent driving potential will occur increases. The form of the relationship between interval and probability of a subsequent event occurring is given by integrating the histogram of intervals (Fig. 9*E*). When this was done the relationship between probability and interval was sigmoidal (Fig. 9*F*). The relationship was adequately described by a Boltzmann sigmoidal expression $[1/(1 + e^{-(t-T_{0.5})/K})]$, where the constant $T_{0.5}$ is the time to half-maximum probability and K is a measure of the slope at half-maximum probability.

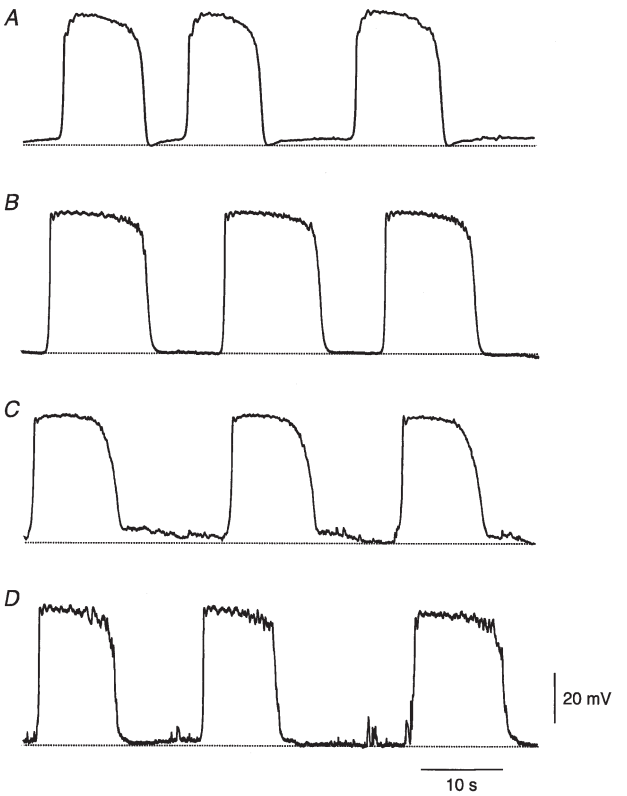

Figure 10. Different forms of driving potentials recorded from ICC_{MY} of guinea-pig antrum

In the example shown in the upper trace (*A*), each driving potential was preceded by a slow depolarization; in this cell the peak negative potential was −68 mV. In the second recording (*B*) the interval between successive driving potentials was flat; in this cell the peak negative potential was −70 mV. Trace *C* shows discharges of driving potentials in a cell where each driving potential was followed by an after-depolarization; in this cell the peak negative potential was −65 mV. The bottom trace (*D*) shows successive driving potentials recorded from a cell in which prominent discharges of unitary potentials were apparent; in this cell the peak negative potential was −65 mV. The time and voltage calibration bars apply to all recordings.

For preparations analysed in this way the mean values of the constants, $T_{0.5}$ and K, were 9.0 ± 0.7 s and 0.78 ± 0.15, respectively ($n = 6$).

When the simultaneous recordings of driving potentials and follower potentials were inspected it was clear that both the variations in half-width and interval detected in driving potentials also occurred in the simultaneous recordings of follower potentials obtained from the longitudinal muscle layer (see Fig. 4). Since the recordings from the muscle layer must reflect activity in many nearby ICC_{MY}, the same variations in time course and interval detected in a single interstitial cell must occur throughout the local population of ICC_{MY}. A point also apparent from Fig. 4*C*, which we noted throughout the experimental series, was that although the duration of individual driving potentials varied greatly, variations in duration were not associated with changes in the shape of the repolarizing phase at the end of each driving potential. Thus in a given preparation, whatever the interval between, or duration of, each driving potential, the time courses of successive decay phases showed little variation other than when interrupted by obvious unitary potentials.

The previous observations have suggested that during the interval between driving potentials, the probability that a subsequent driving potential will occur increases after a delay from a low to a high value. To investigate what might contribute to this increase in probability, the baseline regions between driving potentials were examined. Considerable variability between recordings and even during recordings from a single cell was noted. In general the pattern of the 'diastolic' interval could be divided into four groups. In a proportion of recordings, 17 out of 84 ICC_{MY} examined in 58 different preparations, the interval often lacked obvious discharges of membrane noise and the membrane potential smoothly depolarized until a driving potential was initiated (Fig. 10*A*). In other cells, 34 of 84, the diastolic interval appeared to be flat, lacking obvious discharges of membrane noise with the baseline being abruptly interrupted by the upstroke of a driving potential (Fig. 10*B*). In a further proportion of cells, 21 of 84, each driving potential was followed by an after-depolarization which waned before the initiation of the subsequent driving potential; characteristically an ongoing discharge of membrane noise occurred during the after-depolarization (Fig. 10*C*). In the other group of cells, 12 of 84, discharges of unitary potentials occurred during the diastolic interval (Fig. 10*D*).

It is to be stressed that this subdivision is somewhat arbitrary as in many recordings the pattern of the diastolic interval changed from cycle to cycle. In the recordings shown in Fig. 4, it can be seen that most driving potentials were preceded by a slow diastolic depolarization (Fig. 5*Aa*) whereas others arose abruptly from a flat baseline (Fig. 4*Ab*). Similarly in the four traces

shown in Fig. 11, each selected from a continuous recording from one cell, one diastolic depolarization lacked an obvious discharge of unitary potentials (Fig. 11*Db*). Others displayed diastolic depolarizations with discharges of unitary potentials (Fig. 11*Ab* and *Bb*) whilst another was essentially flat but interrupted by a discharge of unitary potentials (Fig. 11*Eb*).

In eight of the preparations where discharges of membrane noise were apparent, the mean time course of the occurrence of membrane noise was determined. This was done by determining the standard deviation about the mean time course of successive membrane potential recordings, either starting at the ends of each preceding driving potential (Fig. 11*A*, *B* and *C*) or in the interval preceding the upstroke of several driving potentials (Fig. 11*D*, *E* and *F*). The standard deviations for eight successive traces determined as a function of time after or preceding a driving potential, were then calculated to give an index of variability over the 'diastolic' interval. These two approaches had to be undertaken given the variability in separation between individual slow waves. With either analysis it was found that the discharge of membrane noise was not constant during the diastolic interval. After the ends of the driving potentials, the standard deviation of the membrane potential recording had a low value indicating that few unitary potentials were occurring at this time (Fig. 11*C*). As the time after the end of each driving potential increased, so did the standard deviation of the membrane potential, suggesting that the rate of discharge of unitary potentials was increasing. Conversely immediately before the start of driving potential, the standard deviation of the membrane noise was high and fell as the interval before the start of the driving potential was increased (Fig. 11*F*). To assess the change in variability of the membrane noise, lines of best fit were fitted to the standard deviation curves; these had a mean positive gradient of $74.3 \pm 37.6\ \mu V\ s^{-1}$ ($n = 8$).

DISCUSSION

These experiments have shown that the rate of generation of slow waves was not constant but varied around a mean value. This resulted from variations in both the rate of generation and the duration of driving potentials originating in ICC_{MY}. Driving potentials consisted of two components, a primary component and a plateau component. After the end of each plateau component the probability that a subsequent driving potential would occur fell and then gradually increased. During the interval between driving potentials, the rate of occurrence of unitary potentials increased in a proportion of individual

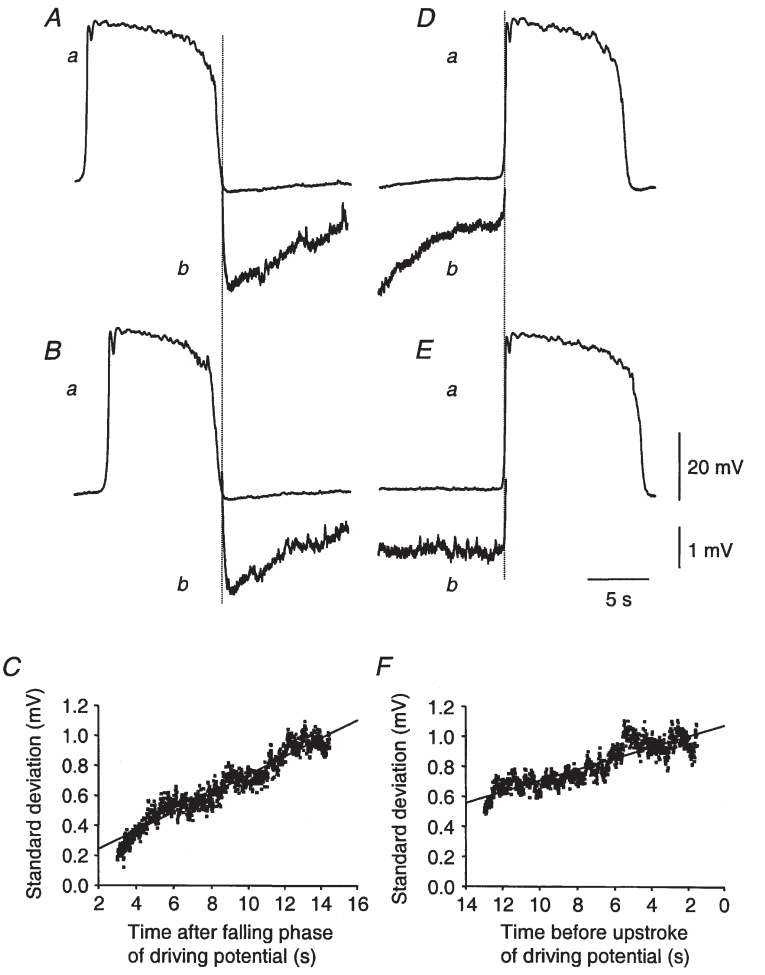

Figure 11. Changes in the discharge of membrane noise during the intervals between driving potentials

Traces *Aa* and *Ba* show two driving potentials followed by the interval before the next driving potential. The 'diastolic' interval is shown at higher gain in *Ab* and *Bb*. The standard deviation about the mean time course calculated during the diastolic interval, recorded after the end of each driving potential, is shown in *C*. It can be seen that the standard deviation was low immediately after the end of the driving potential and steadily increased as the time interval increased. Traces *Da* and *Ea* show two driving potentials along with the interval preceding them; the 'diastolic' interval is shown at higher gain in *Db* and *Eb*. The standard deviation about the mean time course calculated during the diastolic interval, recorded before each driving potential, is shown in *F*. It can be seen that the standard deviation was highest immediately before the occurrence of a driving potential. The time calibration bar applies to all recordings. The upper voltage calibration bar refers to each complete driving potential (*a*), the lower voltage calibration bar applies to the recordings of diastolic interval (*b*).

ICC_{MY}. We suggest that a discharge of unitary potentials triggers a primary component that propagates through the network of ICC_{MY} and activates the plateau component.

Slow waves were first reduced in amplitude and then abolished as progressively higher concentrations of 2APB were applied (Fig. 1). As 2APB has been shown to prevent IP_3-induced Ca^{2+} release (Maruyama *et al.* 1997), the experiments support the view that rhythmical activity in gastrointestinal muscles involves IP_3-dependent release of Ca^{2+} from intracellular stores (Ward *et al.* 2000*b*; Suzuki *et al.* 2000). The observations with 2APB are qualitatively similar to many of those made when a range of caffeine concentrations is applied to these preparations (Tsuengo *et al.* 1995; Dickens *et al.* 1999) and may indicate that caffeine also acts on an IP_3-dependent pathway (Parker & Ivorra, 1991). 2APB in low concentrations, unlike caffeine, initially increased the frequency of slow waves (Fig. 1); one explanation might be that 2APB acts as a partial agonist.

When pacemaker activity involves the sequential activation of voltage-dependent ion channels, the rate of generation of pacemaker activity is quite constant. This is not the case with gastrointestinal muscles where pacemaker activity has a different basis. In the dog colon the discharge of slow waves is irregular; successive slow waves occur at different intervals and have different half-widths (Sanders & Smith, 1986). In dog colon much of this variation results from ongoing neural activity within the enteric nervous system, along with changed eicosanoid production (Sanders & Smith, 1986; Franck *et al.* 1999). However, even when these factors were inhibited, some fluctuations persisted (Sanders & Smith, 1986; Franck *et al.* 1999). In the guinea-pig antrum inhibition of neuronal activity with TTX did not affect the variations in periodicity. The different contributions made by enteric neurones in the two preparations may well result from the different patterns of neural organisation found in the two regions of the gastrointestinal tract (Furness & Costa, 1987).

In intact tissues variations in the rate of generation and duration of driving potentials by ICC_{MY} underlie the fluctuations in periodicity of slow waves (Fig. 2). An irregular discharge of driving potentials continued to occur after the circular muscle layer had been removed (Fig. 4), supporting the view that pacemaker activity is initiated by ICC_{MY} rather than by circular smooth muscle (Dickens *et al.* 1999). Moreover, as the onset of electrical activity in ICC_{MY} coincided with or preceded that detected in the longitudinal smooth muscle layer (Fig. 4), the observations further support the idea that pacemaker activity is initiated by ICC rather than by smooth muscle cells (Thuneberg, 1982; Sanders, 1996). Driving potentials and follower potentials, recorded from preparations with the circular muscle layer removed, had similar time courses and amplitudes to those recorded from the preparations with an intact circular layer (see Dickens *et al.* 1999). It might have been expected that driving potentials, which normally depolarize both the circular and longitudinal muscle layers, would have had greater amplitudes when the electrical load was reduced by removing the circular layer. However, this would not be the case if the peak of the driving potential approached the reversal potential of ionic conductance being activated. This suggests that the reversal potential of the plateau phase is some 40–50 mV positive of the resting potential, i.e. about −20 mV. This value is close to the reversal potential of chloride ions (Cl^-) in many smooth muscles (Aicken & Brading, 1982) perhaps indicating that an increase in Cl^- conductance occurs during the plateau phase. A contribution to pacemaker currents by Cl^- was suggested in the initial study on isolated murine ICC (Tokutomi *et al.* 1995). This view is further supported by the observation that a decrease in the external concentration of Cl^- transiently increases the amplitude of driving potentials recorded from guinea-pig antral ICC_{MY} (Tomita & Hata, 2000; G. D. S. Hirst & F. R. Edwards, unpublished observations). However, it is at odds with the report that non-selective cation channels are primarily responsible for pacemaker depolarizations in cultured murine intestinal ICC_{MY} (Thomsen *et al.* 1998; see Koh *et al.* 1998 for further discussion).

Although ICC_{MY} and longitudinal smooth muscle cells were coupled together into a common electrical syncytium, the signals recorded from them had quite distinct amplitudes (Figs 3 and 4). The difference in amplitude indicates that there must be a relatively high coupling resistance between the syncytial network of ICC_{MY} and the syncytium of smooth muscle cells forming the longitudinal layer. While this point has not been checked directly in these experiments, it has been shown previously that nearby circular smooth muscle cells are better coupled to each other than are nearby ICC_{MY} to circular smooth muscle cells (Dickens *et al.* 1999). Together the observations indicate that the connections between adjacent smooth muscle cells and those between smooth muscle cells and ICC_{MY} are different. This may result from the presence of different connexins in the two sets of gap junctions or from different densities of similar junctions (see Seki *et al.* 1998). Whether this is the case in other regions of the gastrointestinal tract is not clear. In the dog colon, the electrical activity recorded from ICC near the submucosal border (Barajas-Lopez *et al.* 1989) was found to be similar to that recorded in nearby smooth muscle cells (see Sanders & Smith, 1989). On the other hand, large amplitude electrical waves were recorded from what, with hindsight, may well be ICC_{MY} of rabbit intestine (Taylor *et al.* 1975; H. Suzuki & G. D. S. Hirst, unpublished observations). Although isolated intestinal murine ICC_{MY} generate pacemaker waves with amplitudes of some 30 mV and intestinal slow waves have similar amplitudes (Koh *et al.*

1998), recordings have not been made from both cell types *in situ*.

Driving potentials had two components, a primary component and a plateau component. The primary component had a rapid rate of rise and persisted in the presence of caffeine (Fig. 7). The rate of rise and the amplitude of the primary component were reduced and sometimes abolished when $[Ca^{2+}]_o$ was reduced (Fig. 8). The simplest explanation for these observations is that the upstroke of the primary component depends directly on Ca^{2+} entry and it is generated by a set of voltage-dependent calcium channels whilst the plateau involves the release of Ca^{2+} from intracellular stores. Clearly as the primary component was present in the presence of nifedipine, the channels are unlikely to be L-type calcium channels (see also Dickens *et al.* 1999). Although the presence of other voltage-dependent calcium channels has not been described in isolated murine ICC_{MY} (Koh *et al.* 1998), a novel set of voltage-dependent calcium channels was identified in ICC isolated from the pacemaker region of dog colon (Lee & Sanders, 1993). These channels were not blocked by nifedipine, had activation thresholds of −60 to −70 mV and produced transient inward currents (Lee & Sanders, 1993). The inward currents had a total duration of some 100 ms (Lee & Sanders, 1993), a duration much briefer than that of the primary component of the driving potential (Fig. 7). This might indicate that channels like those described by Lee & Sanders (1993) are not involved in the generation of the primary component of antral driving potentials. However, it is not clear what the time course of an action potential sustained by such channels would be, if the action potential were recorded at a point in a network of ICC_{MY} as it propagated through that network.

In contrast to the primary component, the plateau component of the driving potential was abolished by caffeine and was unchanged with moderate reductions in $[Ca^{2+}]_o$ (Figs 7 and 8). The plateau component generated characteristic power spectral-density curves (Fig. 6) with shapes that could be predicted from the time courses of unitary potentials detected in ICC_{MY} (Fig. 5). This implies that the plateau results from an ongoing discharge of many unitary potentials. The power spectral-density curves that were derived from driving potentials generated by ICC_{MY} were strikingly similar to those derived from the regenerative component of the slow wave (Edwards *et al.* 1999). Along these lines, regenerative potentials, triggered in bundles of circular smooth muscle by membrane depolarization, are initiated after a latency of about 1 s (Suzuki & Hirst, 1999). A similar latency precedes the onset of the plateau component of driving potentials (Fig. 7). Both are abolished by caffeine (cf. Fig. 7 with Suzuki & Hirst, 1999). Finally as 2APB abolished all electrical activity in the intact preparations (Fig. 1), both regenerative potentials and driving potentials are likely to involve IP_3-induced Ca^{2+} release. Since the regenerative component of the slow wave appears to originate in smooth muscle bundles (ICC_{IM}) (Dickens *et al.* 2001), the observations suggest that ICC_{MY} and ICC_{IM} have several properties in common. Regenerative potentials in the circular muscle layer have been suggested to result from voltage activation of an IP_3-dependent pathway (Suzuki & Hirst, 1999; van Helden *et al.* 2000), and the plateau component of driving potentials may have a similar basis. The depolarization accompanying the primary component could accelerate IP_3 production (Itoh *et al.* 1992; Ganitkevich & Isenberg, 1993), leading to the increased occurrence of unitary potentials (see Edwards *et al.* 1999). The summation of these potentials would then give rise to a plateau. The alternative possibility that an influx of Ca^{2+} during the primary component might trigger a long lasting discharge of unitary potentials after activating a calcium-induced calcium release pathway seems unlikely; the discharge of slow waves is unaffected by blocking such a pathway with ryanodine (Malysz *et al.* 2001). Clearly further experiments are required to examine the mechanisms underlying the initiation of the plateau component. Any suggestion that ICC_{IM} and ICC_{MY} have similar electrical properties should not be taken to imply that the two sets of cells carry out similar functions within the gastrointestinal tract. ICC_{MY} are the dominant pacemaker cells within the many regions of the gastrointestinal tract (Ward *et al.* 1994; Huizinga *et al.* 1995) and in the stomach lack an inhibitory innervation (Dickens *et al.* 2000). On the other hand, ICC_{IM}, in addition to being involved in the generation of the regenerative component of the slow wave (Dickens *et al.* 2001), invariably receive a dense inhibitory and a dense excitatory innervation (Burns *et al.* 1996; Ward *et al.* 2000*a*). As such, ICC_{IM} are key intermediaries in the processes of neuroeffector transmission in the gastrointestinal tract (Burns *et al.* 1996; Ward *et al.* 2000*a*).

Variations in the rate of generation of driving potentials resulted from variations in both the duration of, and the interval between, successive driving potentials (Fig. 9). As the interval between driving potentials increased, the duration of the subsequent driving potential was also increased. The slopes of the relationship between interval and subsequent duration indicated that each 1 s increase in the interval increased the duration of the subsequent driving potential by some 300 ms. We have no simple explanation for this observation. It is difficult to attribute this behaviour to that of previously described ion-selective membrane channels. One possibility might be that the longer the interval between driving potentials then the greater the synthesis of some messenger involved in the production of the plateau component. Alternatively, longer intervals might allow a more complete filling of an internal store, perhaps with Ca^{2+} ions. Again regenerative potentials recorded from the circular muscle layer of the antrum and driving potentials show similar properties. Regenerative

potentials have an absolute refractory period of some 5 s and a partial refractory period lasting a further 10 to 20 s. During the partial refractory period, the amplitudes of regenerative potentials progressively increase, again suggesting that a slow time-dependent recovery process may limit the size of the responses (Suzuki & Hirst, 1999).

The intervals between successive driving potentials varied from cycle to cycle (Fig. 9). After the end of each driving potential, a subsequent driving potential occurred only after a minimum latency of some 3–5 s (Fig. 9*E*). As the interval increased then the probability that a subsequent driving potential would occur increased (Fig. 9*F*). When the membrane potential changes between pairs of driving potentials were inspected, the form was found to vary from recording to recording (Fig. 10) and often from interval to interval when recording from a single cell (Fig. 11). On some occasions a slow diastolic depolarization preceded the start of a driving potential, on others driving potentials were initiated abruptly from a flat baseline. These observations might indicate that the site of initiation of a driving potential is not fixed; rather it varies, often from cycle to cycle. Furthermore, as the cycle rate is not constant, an invariant initiator of pacemaker activity is unlikely to exist anywhere in the network of ICC_{MY}. In a subset of cells the rate of discharge of unitary potentials increased during the interval between driving potentials (Fig. 11). These might give rise to a steady depolarization in nearby cells which may be a measure of the pacemaker current in ICC_{MY}.

A hypothesis that would explain each of these findings is that immediately after a driving potential, the discharge of unitary potentials within the network of ICC_{MY} falls to a low value. As the interval after the driving potential increases then the frequency of unitary potentials within the network of ICC_{MY} will increase. When sufficient unitary potentials occur more or less synchronously, in an area of the network, threshold potential for the initiation of the primary component is reached. According to this hypothesis, the primary component then serves two functions. Firstly it spreads through the network of ICC_{MY} and gives a co-ordinated wave of depolarization (see Lee & Sanders, 1993). Secondly the wave of depolarization accelerates the initiation of the plateau component of the driving potential. Similarly the hypothesis suggests that unitary potentials also serve two functions. In the interval between driving potentials, their gradual increase in frequency of occurrence provides a pacemaker current. During the plateau component, large numbers of unitary potentials sum to produce a long lasting wave of depolarization.

How then is this hypothesis compatible with previous observations? Firstly it implies that pacemaker activity is dependent upon the cyclic release of Ca^{2+} from IP_3-dependent stores (see Suzuki *et al.* 2000; Ward *et al.* 2000*b*; Fig. 1). Secondly it implies that part of the pacemaker mechanism involves a voltage-dependent step. As such, electrical stimulation should be able to alter the rate of generation of slow waves: this has been shown to be the case with strips of dog antrum (Publicover & Sanders, 1986). Thirdly it implies that single ICC_{MY} might only generate small membrane potential oscillations that correspond to the random discharge of unitary potentials and that pacemaker activity will be more robust as the number of ICC_{MY} participating is increased (see Koh *et al.* 1998). In the absence of the primary component, a plateau component would occur only when the discharge of unitary potentials was sufficiently great to trigger the plateau component: rhythmical activity would persist in ICC_{MY} but would occur at a lower rate (Fig. 8) and be uncoordinated in much the same way as activity occurs in the circular layer after ICC_{MY} have been removed (Suzuki & Hirst, 1999; van Helden *et al.* 2000). The hypothesis also suggests that a pacemaker wave will have a variable point of initiation and this was shown to be the case when the site of initiation of successive gastric slow waves was determined (Alvarez & Mahoney, 1922).

Aickin, C. C. & Brading, A. F. (1982). Measurement of intracellular chloride in guinea-pig vas deferens by ion analysis, ^{36}Cl efflux and microelectrodes. *Journal of Physiology* **326**, 139–154.

Alvarez, W. C. & Mahoney, L. J. (1922). Action current in stomach and intestine. *American Journal of Physiology* **58**, 476–493.

Anderson, K.-E. (1993). Pharmacology of lower urinary tract smooth muscles and penile erectile tissues. *Pharmacological Reviews* **45**, 253–307.

Barajas-Lopez, C., Berezin, I., Daniel, E. E. & Huizinga, J. D. (1989). Pacemaker activity recorded in interstitial cells of Cajal of the gastrointestinal tract. *American Journal of Physiology* **257**, C830–835.

Burns, A. J., Lomax, A. E., Torihashi, S., Sanders, K. M. & Ward, S. M. (1996). Interstitial cells of Cajal mediate inhibitory neurotransmission in the stomach. *Proceedings of the National Academy of Sciences of the USA* **93**, 12008–12013.

Choate, J. K., Edwards, F. R., Hirst, G. D. S. & O'Shea, J. E. (1993). Effects of sympathetic nerve stimulation on the sino-atrial node of the guinea-pig. *Journal of Physiology* **471**, 707–727.

Dickens, E. J., Edwards, F. R. & Hirst, G. D. S. (2000). Vagal inhibitory projections to rhythmically active cells in the antral region of guinea-pig stomach. *American Journal of Physiology – Gastrointestinal and Liver Physiology* **279**, G388–399.

Dickens, E. J., Edwards, F. R. & Hirst, G. D. S. (2001). Selective knockout of intramuscular interstitial cells reveals their role in the generation of slow waves in mouse stomach. *Journal of Physiology*, **531**, 827–833.

Dickens, E. J., Hirst, G. D. S. & Tomita, T. (1999). Identification of rhythmically active cells in guinea-pig stomach. *Journal of Physiology* **514**, 515–531.

Edwards, F. R., Hirst, G. D. S. & Suzuki, H. (1999). Unitary nature of regenerative potentials recorded from circular smooth muscle of guinea-pig antrum. *Journal of Physiology* **519**, 235–250.

Edwards, F. R., Redman, S. J. & Walmsley, B. (1976). Statistical fluctuations in charge transfer at 1a synapses on spinal motoneurones. *Journal of Physiology* **259**, 665–688.

Franck, H., Kong, I. D., Shuttleworth, C. W. & Sanders, K. M. (1999). Rebound excitation and alternating slow wave patterns depend upon eicosanoid production in canine proximal colon. *Journal of Physiology* **520**, 885–895.

Furness, J. B. & Costa, M. (1987). *The Enteric Nervous System*. Churchill-Livingstone, Edinburgh.

Ganitkevich, V. Ya. & Isenberg, G. (1993). Membrane potential modulates inositol 1,4,5-trisphophate-mediated Ca^{2+} transients in guinea-pig coronary myocytes. *Journal of Physiology* **470**, 35–44.

Hirst, G. D. S., Holman, M. E. & Spence, I. (1974). Two types of neurones in the myenteric plexus of duodenum in the guinea-pig. *Journal of Physiology* **236**, 303–326.

Huizinga, J. D., Thuneberg, L., Kluppel, M., Malysz, J., Mikkelsen, H. B. & Bernstein, A. (1995). *W/kit* gene required for interstitial cells of Cajal and for intestinal pacemaker activity. *Nature* **373**, 347–349.

Itoh, M., Seki, N., Suzuki, H., Ito, S., Kajikura, J. & Kuriyama, H. (1992). Membrane hyperpolarization inhibits agonist-induced synthesis of inositol 1,4,5-trisphosphate in rabbit mesenteric artery. *Journal of Physiology* **451**, 307–328.

Koh, S. D., Sanders, K. M. & Ward, S. M. (1998). Spontaneous electrical rhythmicity in cultured interstitial cells of Cajal from the murine small intestine. *Journal of Physiology* **513**, 203–213.

Lee, H. K. & Sanders, K. M. (1993). Comparison of ionic currents from interstitial cells and smooth muscle cells of canine colon. *Journal of Physiology* **460**, 135–152.

Malysz, J., Donnelly, G. & Huizinga, J. D. (2001). Regulation of slow wave frequency by IP_3-sensitive calcium release in the murine small intestine. *American Journal of Physiology – Gastrointestinal and Liver Physiology* **280**, G438–448.

Maruyama, T., Kanaji, T., Nakade, S., Kanno, T. & Mikoshiba, K. (1997). 2APB, 2-aminoethoxydiphenyl borate, a membrane-penetrable modulator of *Ins*(1,4,5)P_3-induced Ca^{2+} release. *Journal of Biochemistry* **122**, 498–505.

Noble, D. (1984). The surprising heart: A review of recent progress in cardiac electrophysiology. *Journal of Physiology* **353**, 1–50.

Ordog, T., Ward, S. M. & Sanders, K. M. (1999). Interstitial cells of Cajal generate electrical slow waves in the murine stomach. *Journal of Physiology* **518**, 257–269.

Parker, I. & Ivorra, I. (1991). Caffeine inhibits inisitol trisphosphate-mediated liberation of intracellular calcium in *Xenopus* oocytes. *Journal of Physiology*, **433**, 229–240.

Publicover, N. G. & Sanders, K. M. (1986). Effects of frequency on the wave form of propagated slow waves in canine gastric antral muscle. *Journal of Physiology* **371**, 179–189.

Sanders, K. M. (1992). Ionic mechanisms of electrical rhythmicity in gastrointestinal smooth muscles. *Annual Review of Physiology* **54**, 439–453.

Sanders, K. M. (1996). A case for interstitial cells of Cajal as pacemakers and mediators of neurotransmission in the gastrointestinal tract. *Gastroenterology* **111**, 492–515.

Sanders, K. M. & Smith, T. K. (1986). Enteric neural regulation of slow waves in circular muscle of the canine proximal colon. *Journal of Physiology* **377**, 297–313.

Sanders, K. M. & Smith, T. K. (1989). Electrophysiology of colonic smooth muscle. In *Handbook of Physiology*, section 6, *The Gastrointestinal Tract*, vol. 1, ed. Schultz, S. G.,Wood, J. D. & Rauner, B. R., pp. 251–271. American Physiological Society, Bethesda, MD, USA.

Seki, K., Zhou, D. S. & Komuro, T. (1998). Immunohistochemical study of the c-*kit* expressing cells and connexin 43 in the guinea-pig digestive tract. *Journal of the Autonomic Nervous System* **68**,182–187.

Suzuki, H. & Hirst, G. D. S. (1999). Regenerative potentials evoked in circular smooth muscle of the antral region of guinea-pig stomach. *Journal of Physiology* **517**, 563–573.

Suzuki, H., Takano, H., Yamamoto, Y., Komuro, T., Saito, M., Kato, K. & Mikoshiba, K. (2000). Properties of gastric smooth muscles obtained from mice which lack inositol trisphosphate receptor. *Journal of Physiology* **525**, 105–111.

Taylor, G. S., Daniel, E. E. & Tomita, T. (1975). Origin and mechanism of intestinal slow waves. In *Proceedings of the 5th International Symposium on GI motility*, ed. VanTrappen, G., pp. 102–106. Typoff Press, Leuven.

Thomsen, L., Robinson, T. L., Lee, J. C., Farraway, L. A., Hughes, M. J., Andrews, D. W. & Huizinga, J. D. (1998). Interstitial cells of Cajal generate a rhythmic pacemaker current. *Nature Medicine* **4**, 848–851.

Thuneberg, L. (1982). Interstitial cells of Cajal: intestinal pacemaker cells? *Advances in Anatomy, Embryology, and Cell Biology* **71**, 1–130.

Tokutomi, N., Maeda, H., Tokutomi, Y., Sato, D., Sugita, M., Nishikawa, S., Nishikawa, S., Nakao, J., Imamura, T. & Nishi, K. (1995). Rhythmic Cl^- current and physiological roles of the intestinal c-*kit*-positive cells. *Pflügers Archiv* **431**,169–177.

Tomita, T. (1981). Electrical activity (spikes and slow waves) in gastrointestinal smooth muscles. In *Smooth Muscle*: *An Assessment of Current Knowledge*, ed. Bülbring, E., Brading, A. F., Jones, A. W. & Tomita, T., pp. 127–156. Edward Arnold, London.

Tomita, T. & Hata, T. (2000). Effects of removal of Na^+ and Cl^- on spontaneous electrical activity, slow wave, in the circular muscle of the guinea-pig gastric antrum. *Japanese Journal of Physiology* **50**, 469–477.

Tsuengo, M., Huang, S.-M., Pang, Y.-W., Chowdhury, J. U. & Tomita, T. (1995). Effects of phosphodiesterase inhibitors on spontaneous electrical activity (slow waves) in guinea-pig gastric muscle. *Journal of Physiology* **485**, 493–502.

van Helden, D. F., Imtiaz, M. S., Nurgaliyeva, K., von der Weid, P. & Dosen, P. J. (2000). Role of calcium stores and membrane voltage in the generation of slow-wave action potentials in guinea-pig gastric pylorus. *Journal of Physiology* **524**, 245–265.

Ward, S. M., Beckett, E. A., Wang, X., Baker, F., Khoyi, M. & Sanders, K. M. (2000*a*). Interstitial cells of Cajal mediate cholinergic neurotransmission from enteric motor neurons. *Journal of Neuroscience* **20**, 1393–1403.

Ward, S. M., Brennan, M. F., Jackson, V. M. & Sanders, K. M. (1999). Role of PI3-kinase in the development of interstitial cells and pacemaking in murine gastrointestinal smooth muscle. *Journal of Physiology* **516**, 835–846.

Ward, S. M., Burns, A. J., Torihashi, S. & Sanders, K. M. (1994). Mutation of the proto-oncogene c-*kit* blocks development of interstitial cells and electrical rhythmicity in murine intestine. *Journal of Physiology* **480**, 91–97.

Ward, S. M., Harney, S. C., Bayguinov, J. R., Mclaren, G. J. & Sanders, K. M. (1997). Development of electrical rhythmicity in the murine gastrointestinal tract is specifically encoded in the tunica muscularis. *Journal of Physiology* **505**, 241–258.

Ward, S. M., Ordog, T., Koh, S. D., Baker, S. A., Jun, J. Y., Amberg, G., Monaghan, K. & Sanders, K. M. (2000*b*). Pacemaking in interstitial cells of Cajal depends upon calcium handling by endoplasmic reticulum and mitochondria. *Journal of Physiology* **525**, 355–361.

Acknowledgements

This project was supported by a grant from the Australian NH & MRC. We are very grateful to Dr Helen Cousins for her helpful comments on the manuscript.

Corresponding author

G. D. S. Hirst: Department of Zoology, University of Melbourne, Victoria 3010, Australia.

Email: d.hirst@zoology.unimelb.edu.au